# Measurements of Turbulent Vertical Kinetic Energy in the Ocean Mixed Layer from Lagrangian Floats

RUO-SHAN TSENG

*Department of Marine Resources, National Sun Yat-sen University, Kaohsiung, Taiwan*

ERIC A. D'ASARO

*Applied Physics Laboratory and School of Oceanography, University of Washington, Seattle, Washington*

(Manuscript received 7 March 2003, in final form 19 March 2004)

ABSTRACT

D'Asaro, in previous work using nearly neutrally buoyant Lagrangian floats in a wind forced mixed layer, found $\langle w^2 \rangle = \overline{A} u_*^2$, where $\langle w^2 \rangle$ is the mean square vertical velocity and $u_*$ is the friction velocity estimated from shipboard meteorological measurements using bulk formulas. Depth profiles of $A(z) = \langle w^2 \rangle(z)/u_*^2$ within the mixed layer showed a maximum value of $A(z)$ of about 2, which is 1.75–2 times that measured in solid-wall turbulent boundary layers driven by a wall stress alone. This result implied that the ocean mixed layer was more energetic than shear-driven turbulent boundary layers driven by the same stress. Here these results are verified using observations of vertical velocity in the mixed layer from 72 float days of data from two Lagrangian floats in the North Pacific Ocean in the autumn of 2000. These floats were more neutrally buoyant than those used previously by D'Asaro, thus reducing possible biases. Wind stress was estimated from Quick Scatterometer satellite measurements and is thus subject to errors and biases different from those in D'Asaro's previous work. Despite these instrumental differences, the new results are very similar to those of the previous work, except that no corrections for internal wave velocities are needed. The values of $\langle w^2 \rangle^{1/2}$ and $u_*$ are correlated well, and the maximum value of $A(z)$ is near 2.

## 1. Introduction

Measurements of the turbulent properties of the upper-ocean boundary layer are very limited. Detailed verification of boundary layer models will require measurements of the usual suite of turbulence statistics: energy and scalar dissipation rates, turbulent kinetic energy, anisotropy, vertical scalar fluxes, and vertical energy fluxes, as well as spectra of these quantities. Of these, only the first is well measured (e.g., Drennan 1996). It seems unlikely that models will be substantially improved without a better characterization of these turbulent properties.

D'Asaro (2001, henceforth D01) describes observations of vertical kinetic energy in a wind-forced upper-ocean mixed layer made using neutrally buoyant Lagrangian floats. Two important results were found: First, a strong correlation existed between the rms vertical velocity $\langle w^2 \rangle$ and the wind stress $u_*^2$. The average ratio of $A = \langle w^2 \rangle / u_*^2$ was 1.75–2 times that found in solid-wall, stress-driven boundary layers, such as the atmospheric boundary layer. In accord with this result, the turbulence properties of such boundary layers cannot be used to calibrate oceanic boundary layer models. Second, no additional correlations between $\langle w^2 \rangle$ and other properties of the ocean or atmosphere were found, including surface wave energy, Stokes drift, wave age, Langmuir number, or surface buoyancy flux. This result is surprising because surface waves undoubtedly play an important role in the boundary layer physics. If both of these results were generally true, they would provide both an important benchmark for model testing and an indication that the effects of surface waves, although important dynamically, can be accurately parameterized in ocean boundary layer models through the wind stress.

In this paper, we describe a different set of Lagrangian-float mixed layer turbulence observations. These floats had a number of differences with and significant improvements over the previous floats. Furthermore, the air–sea fluxes were estimated differently. The use of floats for turbulence measurements is relatively new and is subject to methodological uncertainties. Thus, additional tests of the D01 results are warranted.

*Corresponding author address:* Ruo-Shan Tseng, P.O. Box 59-161, Kaohsiung 804, Taiwan.
E-mail: rstseng@mail.nsysu.edu.tw

© 2004 American Meteorological Society

Unauthenticated | Downloaded 09/13/24 07:05 PM UTC

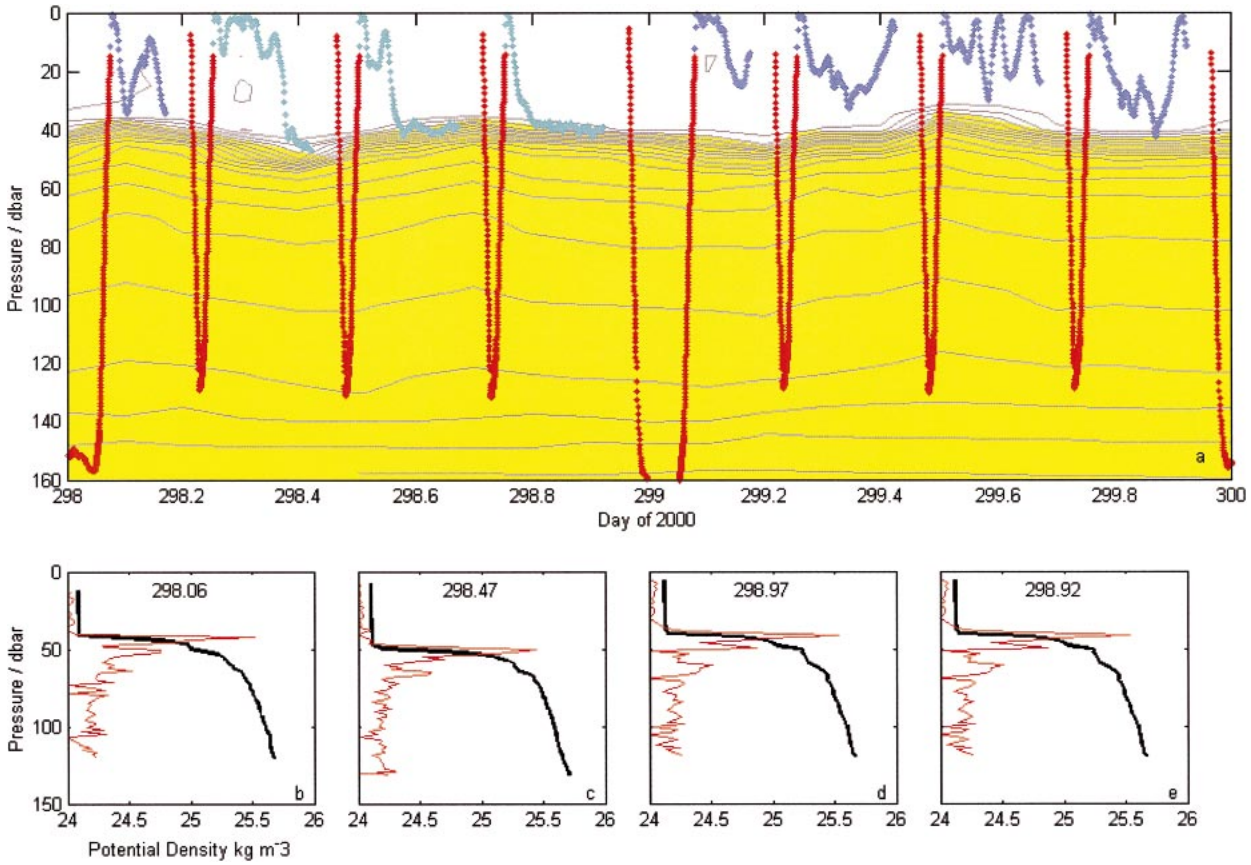


FIG. 1. Examples of float data. (a) Two days of float-7 depth–time data are shown. Profile data are shown by red dots. Lagrangian drift data are shown by blue or cyan dots. Black lines show contours of potential density with a contour interval of 0.1 kg $m^{-3}$. The mixed layer is white; the rest of the domain is yellow. Only float data that remain within the mixed layer are used in the subsequent analysis (blue dots). Lagrangian drift data that are not used in the analysis are shown by cyan dots. (b)–(e) Representative profiles of potential density (black). Time is labeled within each box. Profiles of buoyancy frequency computed from this are shown in red scaled so that a change of 0.01 $s^{-1}$ corresponds to 0.3 kg $m^{-3}$.

## 2. Measurements

### *a. Lagrangian floats*

Two Lagrangian floats (numbers 6 and 7) were deployed in the open North Pacific Ocean (approximately 45.4°N, 147°W) for nearly 40 days: 27 September–7 November 2000 for float 6 and 30 September–1 November 2000 for float 7. Lagrangian floats are designed to follow accurately the three-dimensional motion of the water surrounding them in turbulent flows. This is done through the combination of a density that accurately matches that of the surrounding water and a large drag, which reduces the effect of any residual density difference. The float model used here (''MLFII'') consisted of a cylinder 0.85 m long, 0.25 m in diameter, and 50 L in volume, whose mechanical properties have been adjusted to make its compressibility close to that of seawater. A piston was pushed in and out of the bottom end cap to control the float's buoyancy. A folding cloth drogue, roughly 1 $m^2$ in area, was attached near the bottom of the cylinder to provide extra drag. The float's depth was measured using a pressure sensor. Each float carried two CTDs, one on each end (1.4 m apart). These sensors were used to control the piston and thus the float's density. Detailed discussions of Lagrangian float design, operation, and performance can be found in D'Asaro et al. (1996) and D'Asaro (2003b).

Each day of the mission was divided into four approximately 4-h-long Lagrangian drift periods (Fig. 1a). Between drifts the float profiled to approximately 130 dbar 3 times per day and to approximately 170 dbar once per day. At the top of each profile each float measured its position using GPS or Argos, telemetered this and a subset of its data to shore via the Orbcomm satellite system, and received commands. The vertical resolution during the profiles was 1–2 m.

The mixed layer depth was determined from each density profile (Figs. 1b–d) measured using the lower CTD. The upper CTD often fills with air when the float is near the surface and thus provides poor measurements of salinity in this region. The mixed layer depth was defined as the depth at which the density deviation from

Unauthenticated | Downloaded 09/13/24 07:05 PM UTC

its average value between 15 and 20 dbar was greater than 0.05 kg $m^{-3}$. The four profiles per day allow both tidal and inertial variations in the mixed layer depth to be resolved. Some variability in the mixed layer depth is not resolved, because that depth can, in principle, vary at frequencies up to $N$, the buoyancy frequency. However, the data indicate that this unresolved variability is small. For example, in Fig. 1a, the float falls out of the mixed layer and rests on the top of the thermocline for several drift segments during day 298. The vertical variation of the mixed-layer depth during these times is approximated well by the variation in float depth. The deviation of the float depth relative to the computed mixed layer depth is less than 5 m. Because the mixed layer depth is used only to reject float data that persist below the mixed layer and to scale the float depth, these small errors are insignificant.

The float's potential density was set to match that of the mixed layer at the start of each drift, thus compensating for changes in the mixed layer's temperature and salinity every 6 h. The float density was adjusted every 100 s for changes in float and water density caused by pressure changes. Solar heating of the float is negligible because of the very weak solar radiation and the strong thermal coupling of the aluminum hull to the water. Data were sampled every 100 s. A typical example of float depth–time trajectories and the corresponding mixed layer depth is shown in Fig. 1a.

### b. *How well do the floats measure vertical kinetic energy?*

The float measured vertical velocity from pressure using central differences. Only Lagrangian drift segments for which the float remained above the mixed layer depth were used for estimation of turbulent vertical kinetic energy. Thus, in Fig. 1a, the first and fifth through eighth drift segment were used (blue dots in the figure), but the second, third, and fourth (cyan dots in the figure) were not.

This measurement is nearly free of surface wave contamination because pressure fluctuations are zero along particle paths in linear surface waves and because real surface waves are nearly linear. High-frequency pressure measurements on floats show weak fluctuations at surface-wave frequencies; their magnitude can be explained by the fact that the pressure sensor is mounted somewhat above the center of the float and therefore does not exactly follow a Lagrangian path. D01 and D'Asaro et al. (1996) provide a more extensive discussion of this point.

Numerical studies of ideal Lagrangian particles in simulated turbulent flows (Harcourt et al. 2002; D'Asaro et al. 2002) confirm that these particles can accurately sample the Eulerian turbulent properties of the flow. They also show that imperfectly Lagrangian particles, in particular, those that are buoyant, produce biased measurements of the turbulence. For turbulent boundary layers, the major effect is that buoyant floats tend to remain near the surface until they are carried into the interior by a large downward vertical velocity. Thus, they tend to overestimate the vertical velocity in the layer interior, which was confirmed by D'Asaro (2004) who demonstrated an approximately 10% overestimate of $\langle w^2 \rangle$ in the data of D01 for the most buoyant floats. The effect on the average $\langle w^2 \rangle$ was much less, because most floats were less buoyant. D'Asaro (2004) shows that the floats used in this study better match the density of the mixed layer than those in D01, which should lead to a smaller sampling bias.

Float 6 carried a Doppler sonar that measured the velocity of the float relative to the water in a region approximately 0.2 m above the top of the float. During the Lagrangian drifts, the 2.5-day averaged float velocity varied from $2 \times 10^{-4}$ m $s^{-1}$ downward to $1.2 \times 10^{-3}$ m $s^{-1}$ upward, with an overall mean close to $8 \times 10^{-4}$ m $s^{-1}$. These values are well below the probable bias error in the sonar measurement and are 1/10 or less of the vertical velocity of the float.

The average float buoyancy is difficult to estimate accurately because there is no way to measure it directly in situ. Several factors contribute, however. First, laboratory tests clearly show that the floats have a nonlinear compressibility at low pressure consistent with the presence of a small quantity of air attached to the float. D'Asaro (2003b) uses the Doppler sonar on float 6 to estimate the amount of air as a function of time. It decreased with an $e$-folding time of about 4 days from about 20 $cm^3$ at atmospheric pressure when the float is first deployed, down to negligible amounts after about 10 days. Second, all Lagrangian floats slowly gain weight with time through an unknown reaction of anodized aluminum with seawater (D'Asaro 2004). This effect is minimized in these data because the float is programmed to settle to its own density level once per day and uses this information to recompute its own density. Third, an error in tracking the piston position caused an offset in the float's buoyancy with a period of 5 days and a maximum magnitude of about 5 g too heavy. During the heavy phase, the floats often fell out of the mixed layer, thus eliminating this drift segment from the analysis. Based on this alone, the average buoyancy of the floats within the mixed layer would be about 2 g too heavy, with a variability of about $\pm 2$ g. However, during the mission, the overall buoyancy of the float was increased by command to make the depth distribution within the mixed layer nearly uniform and to minimize the times that the float settled below the mixed layer. Thus, the best guess is that the average float buoyancy was nearly zero, with a variation of $\pm$ 2 g due to the tracking error. Using a normal quadratic drag law [see D'Asaro (2003b) for a discussion of drag] and a drogue area of 0.8 $m^2$, this buoyancy implies a net motion relative to the water of $\pm 0.005$ m $s^{-1}$, a value very close to that estimated from the sonar.

Other errors in the ability of floats to sample turbu-

Unauthenticated | Downloaded 09/13/24 07:05 PM UTC

lence can result from their shape and finite size. The floats are clearly larger than the smallest scales of turbulence. They therefore cannot follow water molecules, but must follow the average velocity of the water surrounding them. Lien et al. (1998) address this problem for fully turbulent flows and derive a response function that describes the high-frequency attenuation of the Lagrangian frequency spectrum for finite-sized floats. This function is found to fit accurately the spectra measured by floats in such flows. For boundary layer turbulence, the effect on the estimation of kinetic energy is small if the boundary layer is significantly larger than the floats. For the data presented here, the finite size of the floats will reduce the kinetic energy that they measure by an estimated 5% in the middle of the boundary layer.

One can also imagine that the floats could have lift in a sheared flow and that this lift would cause them to be non-Lagrangian. These effects are difficult to estimate accurately. The shear velocity relative to the float, from above, should be about 10% of the total velocity, or a few millimeters per second. The resulting motion of the float relative to the water should be even smaller because the lift velocity cannot be larger than the total. These velocities are smaller than the motion of the float relative to the water due to buoyancy, and their net effect on the estimates of kinetic energy should therefore be quite small.

### *c. Air–sea fluxes*

#### 1) HEAT FLUX

Determination of the air–sea heat flux is not crucial to the data analysis, serving only to verify that the mixed layer turbulence is primarily wind driven. Thus, for the purposes of this note, relatively inaccurate estimates of air–sea heat flux will suffice.

Josey et al. (1999) compute the climatological mean net air–sea heat flux for October and November at this location as $-30$ and $-80$ W m$^{-2}$, respectively. D'Asaro (2003a) describes how the vertical velocity and temperature measurements on floats can be used to compute the surface heat flux using a covariance method. D'Asaro (2004) compares this method with bulk flux estimates and finds accuracies of better than 10 W m$^{-2}$. Using this method with these data, the surface heat flux over 5-day intervals was computed. It ranges from about 50 (heating) to about $-100$ W m$^{-2}$ (cooling), with an average of about $-60$ W m$^{-2}$. In response, the mixed layer cooled from about 18.2° to 13.4°C at float 7 and from 18.2° to 12.2°C at float 6. As is usual in this area (Large 1996), about one-half of the cooling was due to entrainment of cold water from below as the mixed layer deepened.

#### 2) WIND STRESS

Wind stress measurements were made using wind speeds from the Quick Scatterometer (QuikSCAT) satellite. Previous studies have shown scatterometer winds to be reliable and accurate. Comparisons of National Aeronautics and Space Administration Scatterometer (NSCAT) data with data from the National Data Buoy Center (NDBC) buoys indicate that the NSCAT wind speeds have an rms error of 1.3 m s$^{-1}$ for wind speeds from 3 to 17 m s$^{-1}$ (Freilich and Dunbar 1999; Austin and Pierson 1999). A similar analysis using QuikSCAT winds yields an rms error of 1.01 m s$^{-1}$ (Ebuchi et al. 2002).

QuikSCAT winds adjusted to 10-m height and neutral stability for a $2° \times 2°$ region around each float location at a resolution of 25 km were acquired from the QuikSCAT surface wind retrieval Internet site of the Department of Atmospheric Sciences, University of Washington (http://pbl.atmos.washington.edu/). At least two QuikSCAT passes were usually available for each day, one in the morning and one in the evening. The QuikSCAT vectors were first screened for contamination by precipitation. The float position at the time of each QuikSCAT pass was determined from interpolations of the float trajectories. The wind vectors at these float locations at the QuikSCAT pass times were then spatially interpolated from the neighboring QuikSCAT winds by the inverse-distance method (Emery and Thomson 1998). Wind stress was calculated by assuming neutral stratification after the method of Large and Pond (1981). No corrections for sea surface velocity are necessary with QuikSCAT data because microwave scattering is unaffected by it. Kelly et al. (2001) show that the wind stress computed from QuikSCAT data clearly correlates much better with buoy stress computed from the difference between the air and the water velocities when compared with stress computed from the wind alone. No corrections for atmospheric boundary layer stratification are necessary because QuikSCAT winds are corrected to neutral stratification (Li et al. 1989; Ebuchi et al. 2002).

## 3. The setting

These measurements were made in a region of relatively strong wind forcing and very weak mesoscale eddies. Surface drifter trajectories in this region can be accurately predicted from the wind stress and historical geostrophic currents alone (Ingraham and Miyahara 1988). During the D01 measurements, horizontal gradients in the mixed layer lead to rapid restratification of the mixed layer during periods of weak winds. This effect is much weaker at this location. At both locations, storms generated large inertial oscillations, which lead to intermittent strong cooling of the mixed layer by entrainment of water from below. Only a very weak diurnal temperature signal, less than 0.1°C, is present. This signal is barely resolvable above the turbulent temperature fluctuations in the mixed layer.

Figure 2 shows the wind direction, wind speed, and mixed layer depth as determined from the QuikSCAT

Unauthenticated | Downloaded 09/13/24 07:05 PM UTC

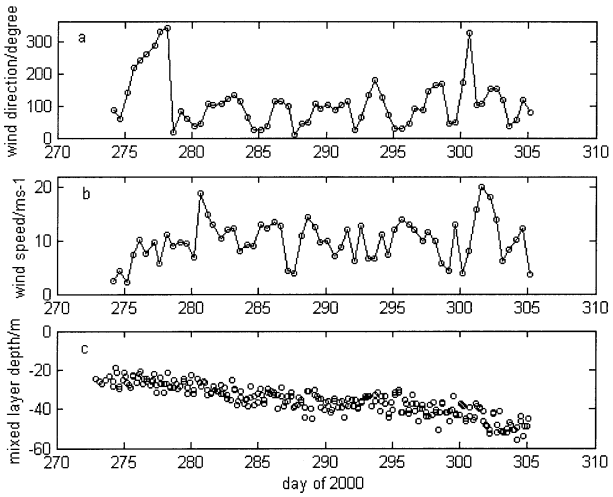


FIG. 2. (a) QuikSCAT wind direction and (b) wind speed at float-7 locations and (c) the corresponding mixed layer depth along the float trajectory.

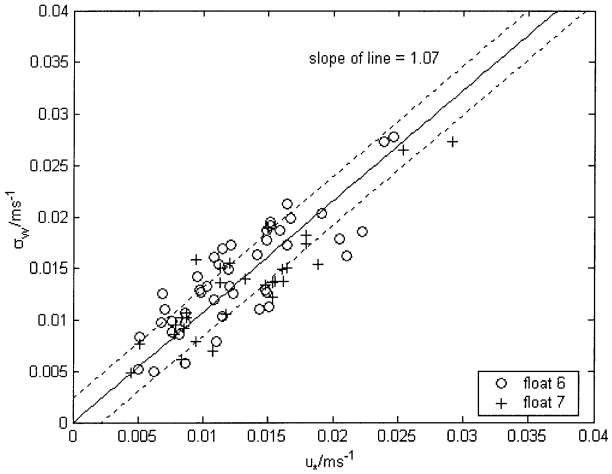


FIG. 3. Root-mean-square vertical velocity $\langle w^2\rangle^{1/2}$ as a function of friction velocity $u_*$ for Lagrangian float data within the mixed layer. The line has a slope of 1.07. The dotted lines indicate 1 standard deviation of measurement error in $u_*$.

and float data, respectively. The winds generally blew toward the northeast or east (Fig. 2a), and the wind speed increased, on average, from about 2 m $s^{-1}$ at day 274 to a maximum wind speed of about 21 m $s^{-1}$ at day 302 (Fig. 2b). Surface trajectories of both floats (not shown here) show them moving in a generally downwind direction with horizontal velocities of no more than 0.7 m $s^{-1}$. The mixed layer depth increased gradually from 20 to nearly 60 m (Fig. 2c). Density profiles (Fig. 1b) indicate that the mixed layers were generally well mixed and that the average potential density in the mixed layer increased from 23.3 to 24.4 kg $m^{-3}$.

## 4. Analysis and results

### *a. Correlation with wind stress*

The vertical velocity variance $\langle w^2\rangle$ was estimated from the 3.7-h average of float vertical velocities. Typical float vertical velocities were 0.01–0.03 m $s^{-1}$, with the maximum vertical velocity of 0.06 m $s^{-1}$. Typical overturning times were 0.5–1 h. Therefore, during the averaging time of $\langle w^2\rangle$ the float traverses the mixed layer several times. Values of $\langle w^2\rangle$ that occurred within 6 h of a QuikSCAT wind estimate were grouped with the wind stress from that estimate. A total of 75 sets of $\langle w^2\rangle$ and $u_*^2$ were obtained, 45 from float 6 and 30 from float 7. A scatterplot (Fig. 3) indicates a clear linear relationship with the ratio $\langle w^2\rangle^{1/2}/u_* = \overline{A}^{1/2} = 1.07 \pm 0.05$, where the error represents two standard deviations of the mean calculated from the standard deviation of $\langle w^2\rangle^{1/2}/u_*$ assuming 75 independent wind stress estimates. The value of $A$, 1.14 $\pm$ 0.06, is slightly smaller than the value 1.35 $\pm$ 0.07 reported by D01 (D01, his Fig. 4).

Random deviations from the linear relationship in Fig. 3 can be attributed to statistical variations and measurement errors from using the QuikSCAT winds. A single value of QuikSCAT wind speed is used to define $u_*$ for 12 h of float data. Estimates of the resulting errors were obtained using wind measurements at the nearest NDBC buoy (46006; 40.80°N, 137.48°W) for October, November, and December of 2000. Estimates of $u_*$ in a 12-h window have an rms deviation of about 0.0016 m $s^{-1}$ from their value at the center of the window. Combining this estimate with a QuikSCAT wind error of 1.3 m $s^{-1}$ results in an rms error in $u_*$ of 0.0022 m $s^{-1}$. This range, drawn as the dashed lines in Fig. 3, clearly encompasses the observed variation in the scatterplot.

Systematic errors are small. Sensitivity tests for the QuikSCAT rain flag, the averaging time interval, the wind stress bulk formulas, and the separation length between the QuikSCAT and drift times were made. The linear relationship between $\langle w^2\rangle^{1/2}$ and $u_*$ in Fig. 3 remains consistent under these variations, and the slope of the best-fit line varies by only 2.8%.

### *b. Depth variation*

Figure 4 plots the probability distribution of float data as a function of $z/H$ (solid bars). The distribution is nearly uniform from the surface down to a depth of about $0.6H$ and is more uniform than that of D01 (cf. with D01's Fig. 6). As discussed in D'Asaro (2003b), this result indicates that the floats used here are more neutrally buoyant and thus more accurately Lagrangian than those used in D01.

The scaled vertical kinetic energy $A(z)$ is plotted in Fig. 4 as a function of the scaled depth $z/H$, where $H$ is the mixed layer depth. In comparing with Fig. 6 of D01, it is seen that both rise to a maximum of about 2 in the upper part of the mixed layer. The depth of the maxima is slightly deeper here; $z/H = 0.3$ rather than

Unauthenticated | Downloaded 09/13/24 07:05 PM UTC

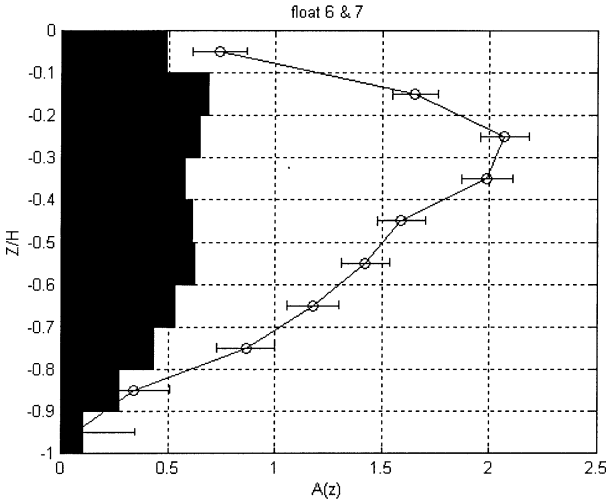


FIG. 4. Scaled vertical kinetic energy $A(z) = \langle w^2 \rangle / u_*^2$ as a function of scaled depth $z/H$. Error bars are 1 standard deviation of the mean in each bin. Black bars indicate probability distribution of float data on an arbitrary scale.

0.2. Both decrease from the maximum to the mixed layer base. In D01, the $A(z)$ profile did not go to zero at the mixed layer base. This was attributed to the presence of internal waves, and a correction was made to remove this effect. Here, no such correction was necessary. The mixed layer average of $A(z)$ is 1.19, very close to the time average value of 1.14 as obtained from Fig. 3 and somewhat higher than the value of about 1.0 for the corrected profile in D01.

### c. Contribution from buoyancy flux

The contribution of buoyancy flux $J_b$ to $\langle w^2 \rangle$ is small for two reasons. First, the buoyancy flux contributed by the air–sea heat flux is small. Using $J_b = g\alpha Q_0 / \rho C_p$, where $\alpha = 2.1 \times 10^{-4}$ °C$^{-1}$ is the thermal expansion coefficient of seawater, $Q_0 = 100$ W m$^{-2}$ is the heat flux, $\rho C_p = 4.1 \times 10^{-6}$ J °C$^{-1}$ m$^{-3}$ is the heat capacity, and $g$ is the acceleration of gravity, $J_{b0} = 5 \times 10^{-8}$ m$^2$ s$^{-3}$. Steffen and D'Asaro (2002) find that for a convectively driven mixed layer $w_{\rm rms} = 0.5(J_b H)^{1/3}$. For the data here, $H = 40$ m, yielding $w_{\rm rms} = 5.8$ mm s$^{-1}$, which is relatively small as compared with the observed $w_{\rm rms}$. Second, this effect is further reduced because the entrainment flux at the base of the mixed layer, computed as in D'Asaro (2004), is generally as large as the surface heat flux, so that the net work done by the buoyancy flux is small or possibly negative.

## 5. Summary and discussion

D01 found a remarkably strong correlation between vertical kinetic energy in the upper-ocean mixed layer and the bulk wind stress. The magnitude of the kinetic energy was approximately 2 times that found in solid-wall, shear-driven boundary layers for the same stress. The purpose of this article was to repeat this analysis with different data.

Two neutrally buoyant floats were deployed in the North Pacific from late September to early November of 2000. The wind stress field was estimated from the QuikSCAT neutral wind using bulk formulas. A linear relationship between the wind stress and the vertical kinetic energy was found. Deviations from this relationship could be entirely explained by the uncertainties in the measurements. The depth profile of the relationship between vertical kinetic energy and wind stress within the mixed layer was very similar to that found by D01, with $A(z) = \langle w^2 \rangle(z)/u_*^2$ reaching a value of 2 at middepth in the mixed layer.

These observations differed from those of D01 in several ways. The density of the floats more closely matched that of the mixed layer, as is apparent in the more uniform vertical distribution of float position. These measurements of $\langle w^2 \rangle$ are therefore more accurate. The wind stress estimates from QuikSCAT were much less frequent than the ship-based estimates used in D01. Resulting interpolation errors caused the measurements of wind stress to be less accurate. The environment also differed. The climatological mixed layer was deeper (70–80 m) for D01, but the turbulent mixing layer varied rapidly in depth because of restratification between wind events. Here, the mixed layer steadily deepened from 20 to 50 m. In D01, the profile of $A(z)$ did not go to zero at the mixed layer base; this was attributed to internal wave energy and required a correction. No such correction was required here. Nevertheless, the two observations have many features in common. Both were conducted in open-ocean, wind-forced boundary layers with relatively mature waves and little mesoscale variability. The results are almost identical quantitatively, supporting the hypothesis that under these conditions wind stress is an excellent predictor of turbulent kinetic energy in the upper-ocean boundary layer.

*Acknowledgments.* RST was supported by the National Science Council of the Republic of China (Grant 40097F) while taking sabbatical leave at the Applied Physics Laboratory, University of Washington, for six months during 2002. EAD was supported by National Science Foundation Grant OCE0117411. We thank Ren-Chieh Lien for his help. The Department of Atmospheric Sciences, University of Washington, kindly provided us the QuikSCAT data.

REFERENCES

Austin, S., and W. J. Pierson, 1999: Mesoscale and synoptic-scale effects on the validation of NSCAT winds by means of data buoy reports. *J. Geophys. Res.*, **104,** 11 437–11 448.

D'Asaro, E. A., 2001: Turbulent vertical kinetic energy in the ocean mixed layer. *J. Phys. Oceanogr.,* **31,** 3530–3537.

——, 2003a: The ocean boundary layer below Hurricane Dennis. *J. Phys. Oceanogr.,* **33,** 561–579.

Unauthenticated | Downloaded 09/13/24 07:05 PM UTC

——, 2003b: Performance of autonomous Lagrangian floats. *J. Atmos. Oceanic Technol.,* **20,** 896–911.
——, 2004: Air–sea heat flux measurements from nearly neutrally buoyancy floats. *J. Atmos. Oceanic Technol.,* **21,** 1086–1094.
——, D. M. Farmer, J. T. Osse, and G. T. Dairiki, 1996: A Lagrangian float. *J. Atmos. Oceanic Technol.,* **13,** 1230–1246.
——, K. B. Winters, and R. C. Lien, 2002: Lagrangian analysis of a convective mixed layer. *J. Geophys. Res.,* **107,** 3040, doi: 10.1029/2000JC000247.
Drennan, W. M., 1996: Ocean turbulence dissipation measurements in SWADE. *J. Phys. Oceanogr.,* **26,** 808–815.
Ebuchi, N., H. C. Graber, and M. J. Caruso, 2002: Evaluation of wind vectors observed by QuikSCAT/SeaWinds using ocean buoy data. *J. Atmos. Oceanic Technol.,* **19,** 2049–2062.
Emery, W. J., and R. E. Thomson, 1998: *Data Analysis Methods in Physical Oceanography.* Pergamon, 634 pp.
Freilich, M. H., and R. S. Dunbar, 1999: The accuracy of the NSCAT-1 vector winds: Comparisons with National Data Buoy Center buoys. *J. Geophys. Res.,* **104,** 11 231–11 246.
Harcourt, R. R., E. L. Steffen, R. W. Garwood, and E. A. D'Asaro, 2002: Fully Lagrangian floats in Labrador Sea deep convection: Comparison of numerical and experimental results. *J. Phys. Oceanogr.,* **32,** 493–510.
Ingraham, W. J., and R. K. Miyahara, 1988: Ocean surface current simulations in the North Pacific Ocean and Bering Sea (OSCURS-Numerical Model). NOAA Tech. Rep. NMFS F/NWC-130, 162 pp.
Josey, S., E. Kent, and P. Taylor, 1999: New insights into the ocean heat budget closure problem from analysis of the SOC air–sea flux climatology. *J. Climate,* **12,** 2856–2880.
Kelly, K. A., S. Dickinson, M. J. McPhaden, and G. C. Johnson, 2001: Ocean currents evident in satellite wind data. *Geophys. Res. Lett.,* **28,** 2469–2472.
Large, W. G., 1996: An observational and numerical investigation of the climatological heat and salt balances at OWS P. *J. Climate,* **9,** 1856–1876.
——, and S. Pond, 1981: Open ocean momentum flux measurements in moderate to strong winds. *J. Phys. Oceanogr.,* **11,** 324–336.
Li, F., W. G. Large, W. Shaw, E. Walsh, and K. Davidson, 1989: Ocean radar backscatter relationship with near surface winds: A case study during FASINEX. *J. Phys. Oceanogr.,* **19,** 342–353.
Lien, R.-C., E. D'Asaro, and G. Dairiki, 1998: Lagrangian frequency spectra of vertical velocity and vorticity in high-Reynolds-number oceanic turbulence. *J. Fluid Mech.,* **362,** 177–198.
Steffen, E., and E. D'Asaro, 2002: Deep convection in the Labrador Sea as observed by Lagrangian floats. *J. Phys. Oceanogr.,* **32,** 475–492.

Unauthenticated | Downloaded 09/13/24 07:05 PM UTC